Chem Soc Rev

Chemical Society Reviews

www.rsc.org/chemsocrev

Volume 41 | Number 24 | 21 December 2012 | Pages 7965–8216

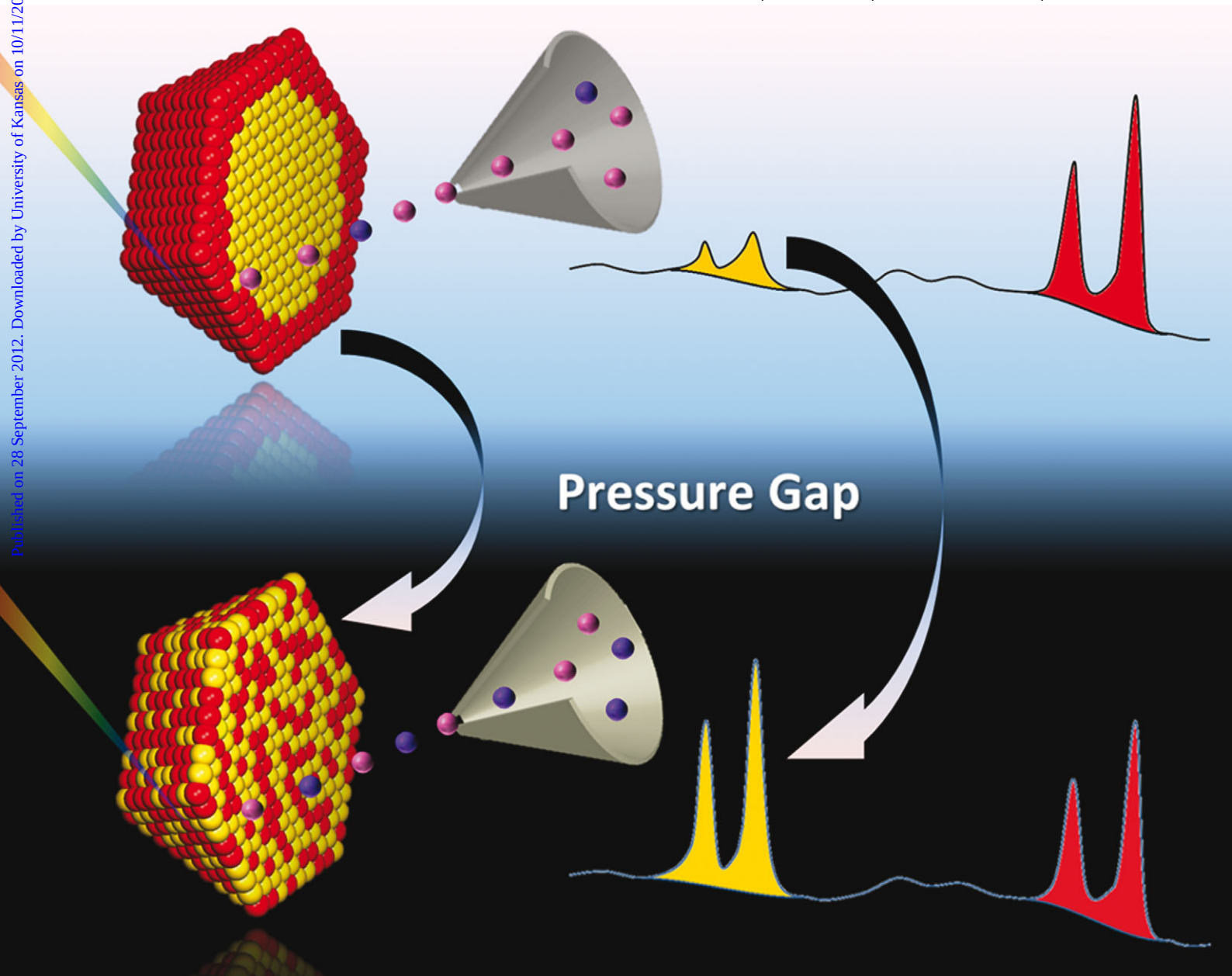

Themed issue: Bimetallic nanocatalysts and nanocatalysis

ISSN 0306-0012

Guest editor: Franklin (Feng) Tao

TUTORIAL REVIEW

Franklin (Feng) Tao, Shiran Zhang, Luan Nguyen and Xueqiang Zhang
Action of bimetallic nanocatalysts under reaction conditions and during catalysis: evolution of chemistry from high vacuum conditions to reaction conditions

RSC Publishing

0306-0012(2012)41:24;1-6

Chem Soc Rev

Cite this: *Chem. Soc. Rev.*, 2012, **41**, 7980–7993

www.rsc.org/csr

TUTORIAL REVIEW

Action of bimetallic nanocatalysts under reaction conditions and during catalysis: evolution of chemistry from high vacuum conditions to reaction conditions†

Franklin (Feng) Tao,* Shiran Zhang, Luan Nguyen and Xueqiang Zhang

Received 22nd May 2012
DOI: 10.1039/c2cs35185d

Bimetallic catalysts are one of the main categories of metal catalysts due to the tunability of electronic and geometric structures through alloying a second metal. The integration of a second metal creates a vast number of possibilities for varying the surface structure and composition of metal catalysts toward designing new catalysts. It is well acknowledged that the surface composition, atomic arrangement, and electronic state of bimetallic catalysts could be different from those before a chemical reaction or catalysis based on *ex situ* studies. Thanks to advances in electron-based surface analytical techniques, the surface chemistry and structure of bimetallic nanoparticles can be characterized under reaction conditions and during catalysis using ambient pressure analytical techniques including ambient pressure XPS, ambient pressure STM, X-ray absorption spectroscopy and others. These ambient pressure studies revealed various restructurings in the composition and arrangement of atoms in the surface region of catalysts under reaction conditions or during catalysis compared to that before reaction. These restructurings are driven by thermodynamic and kinetic factors. The surface energy of the constituent metals and adsorption energy of reactant molecules or dissociated species on a metal component are two main factors from the point of view of thermodynamics. Correlations between the authentic surface structure and chemistry of catalysts during catalysis and simultaneous catalytic performance were built for understanding catalytic mechanisms of bimetallic catalysts toward designing new catalysts with high activity, selectivity, and durability.

1. Introduction

The design of new catalysts is the main driving force in the critical field of heterogeneous catalysis, which is the foundation of energy conversion.[1] Bimetallic materials are important catalysts due to their numerous advantages.[2–7] For example, composition (at large scale), coordination environment of the metal atom (on the atomic scale), and electronic state of the parent metal can be tuned systematically due to the spectacular success in the synthesis of bimetallic nanoparticles in the recent decade.[8–13] As heterogeneous catalysis is performed on the surface of a catalyst, the surface structure and chemistry of a bimetallic catalyst in term of geometric and electronic structures of metal atoms on the surface are the most important parameters which determine the catalytic performance of a bimetallic catalyst.

It is well acknowledged that the differences in catalytic behavior between bimetallic catalysts and monometallic catalysts or between two bimetallic catalysts with different compositions and structures result from two effects: electronic and geometric effects. The electronic effect is also called the ligand effect since the replacement of metal atoms ***A*** coordinating to a target atom ***A*** by metal atoms ***B*** must vary the electronic structure of the target atom ***A*** and thus modify the adsorption energy of a reactant molecule on ***A***. One example is the partial replacement of Pd atoms coordinating to a target Pd atom with Zn atoms formed from reduction of ZnO on the substrate which increases the electron density in the 4d shell of Pd and thus increases the back donation of electrons from the 4d shell to the anti-π bond of CO and thus increases the binding of CO molecules on Pd, which promotes the selectivity to the production of CO_2 and H_2 in methanol steam reforming.[14,15] On the other hand, partial replacement of metal atoms bonded to a parent atom ***A*** with atoms ***B*** offer different binding configurations. Reactant molecules or a dissociated species could favor or even require a specific binding site (on-top site, bridge site, hollow site, or site of monomer pair, *etc.*). Partial replacement of atom A with B could offer a specific binding site which is favorable for one of the reaction channels. Thus, selectivity to the product of this channel can be promoted. One example is that a replacement of Au atoms of Au(100) with Pd forms a specific site consisting of

Department of Chemistry and Biochemistry, University of Notre Dame, Notre Dame, Indiana 46556, USA. E-mail: ftao@nd.edu; Tel: +1 574 631 1394
† Part of the bimetallic nanocatalysts themed issue.

a pair of Pd monomers with a distance favorable for the coupling of two critical surface species, acetate and ethylic species to form vinyl acetate.[16] This alloy catalyst significantly promotes the production of vinyl acetate. However, in many cases it is challenging to distinguish a change in electronic structure and geometric effect since the formation of a geometrically favorable binding site is accompanied by an electronic effect.

Similar to other chemical processes performed at the interface of two phases, heterogeneous catalysis is always performed at an interface of a solid catalyst and gaseous or liquid reactants around it. However, reaction conditions for catalysis are typically ambient or high temperatures of catalysts in an environment of reactants at ambient or high pressure. In reactive or corrosive environments (reactive gases or liquids, acidic solutions, *etc.*), the surfaces of most materials are likely to restructure, adapting their geometrical and electronic structures to the surroundings in terms of gaseous or liquid reactants.[5,17–28] Such changes in surface structure and chemistry have profound effects on the function of materials. In many cases, the structure and composition of the material surface in the reactive (or corrosive) environment in which it functions differ markedly than that in a high vacuum environment (the operational environment of most conventional electron-based analytical techniques such as XPS, TEM, SEM...). This difference, generally termed as a restructuring, has been demonstrated using ambient pressure spectroscopy and microscopy techniques.[18] The potential difference in surface structure and chemistry of heterogeneous catalysts between *in situ* and *ex situ* studies is the restructuring processes in catalysis. In addition, the restructurings are performed during other chemical processes of catalysis including pretreatment, deactivation, poisoning *etc.*

A restructuring of a catalyst surface is very likely for bimetallic catalysts. Surface chemistry and structure of catalysts under reaction conditions (typically refers to a reactant gas) or during catalysis (typically an appropriate gas mixture with certain composition of a catalytic reaction) could be very different than those in a clean environment (typically high vacuum or ultra-high vacuum) at room temperature or lower temperatures.

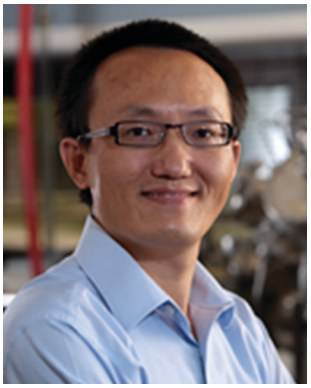

Franklin (Feng) Tao

Franklin (Feng) Tao joined the Department of Chemistry and Biochemistry at University of Notre Dame as a tenure-track assistant professor in 2010 after obtaining a PhD in chemistry from Princeton University followed by a postdoctoral fellowship at Lawrence Berkeley National Lab and University of California at Berkeley. He is currently leading a research group interested in catalysis, energy science, and nanoscience. His group synthesizes nanocatalysts and performs operando and in situ studies of catalytic reactions of different types of hydrogen generation and conversion of greenhouse gases using in-ambient pressure XPS and ambient pressure STM available in his group. He has published about 70 research peer-reviewed articles in international journals and two books by Wiley. He serves on the advisory board of a few journals including Chemical Society Reviews and Catalysis Science and Technology.

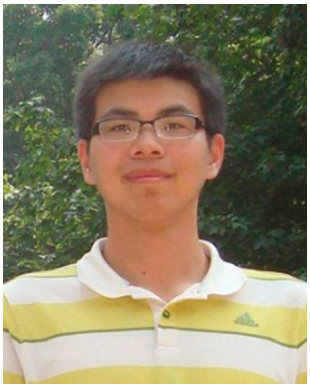

Shiran Zhang

Shiran Zhang is a graduate student of University of Notre Dame. He obtained his BSc in chemistry from University of Science and Technology of China in 2011. He research interest is synthesis of nanomaterials, energy-related catalysis, and characterization of catalysts using ambient pressure techniques.

Luan Nguyen

Luan Nguyen is a graduate student at the Department of Chemistry and Biochemistry at University of Notre Dame. He obtained his BSc in Chemistry from Grand Valley State University in 2011. He works on preparation of bimetallic nanocatalysts and in situ and operando studies of surface chemistry and structure of nanocatalysts.

Xueqiang Zhang

Xueqiang Zhang is a graduate student of University of Notre Dame. He obtained his BSc in chemistry from Jilin University in 2010. His research interest is synthesis of nanomaterials, energy-related catalysis, and characterization of catalysts using ambient pressure techniques.

Although surface structure and chemistry of bimetallic catalysts and the structure and chemistry of bulky bimetallic materials have been well studied in the past decades,[29] it is inappropriate to simply extrapolate the insights obtained under high vacuum at room temperature or lower to predict the surface structure and chemistry of bimetallic catalysts under reaction conditions or during catalysis. One potential difference is the behavior of segregation. Although the difference in surface composition of a metal ***A*** or ***B*** between the surface layer and bulk was reported and termed segregation of bimetallic catalysts in *ex situ* studies, typically observed upon annealing in UHV, a massive restructuring under reaction conditions and during catalysis was reported very recently by using a relatively new surface analytical technique, synchrotron-based ambient pressure electron spectroscopy.[5,17–28]

One of the obvious differences is the oxidation state of a metal element ***A*** or ***B*** under reaction conditions or during catalysis in contrast to that in high vacuum. These differences in surface chemistry and structure are driven by a complicated interplay of *thermodynamic factors*, such as surface energies of metals, binding strengths of each metallic component with adsorbed atoms and molecules, and the tendency of the constituent metal components to form ordered alloy phases, and *kinetic factors*, mainly diffusion barriers of metal atoms. In addition, the size of bimetallic catalysts is also a factor in restructuring since the fraction of atoms with low-coordination (such as atoms at step edges or corners) is higher for smaller nanoparticles.

Studies of the surface structure of catalysts under reaction conditions or during catalysis will reveal the evolution in surface composition and structure of as-synthesized catalysts to the actual surface composition during catalysis. Thus, a direct correlation *between* actual surface composition *and* catalytic performance (activity, selectivity, deactivation, and poisoning effect) can be built. This correlation is the critical insight for understanding catalysis, designing and optimizing catalysts. To build such a correlation, the surface structure and chemistry of bimetallic catalysts under reaction conditions or during catalysis are the critical information.

In this article, we will review the restructuring of bimetallic nanocatalysts during catalysis or under reaction conditions in contrast to the surface structure and chemistry *ex situ*. It is organized by first briefly introducing ambient pressure techniques for studying surface structure and chemistry under reaction conditions or during catalysis (Section 3), and then reviewing restructuring of different bimetallic nanocatalysts (Section 4). Understanding the driving forces of restructurings revealed under reaction conditions or during catalysis is the central topic of this review.

2. Synthesis and preparation of bimetallic nanoparticles

For the purpose of fundamental studies of catalysis, bimetallic nanocatalysts are synthesized with two quite differently methods: wet chemistry and dry chemistry. In terms of wet chemistry, reduction of two metal salts in a solution in a controllable manner is the main approach. Due to the fabulous success in the synthesis of metal nanomaterials in the past decades,[8,30–34] various bimetallic nanomaterials (in most cases, nanoparticles) can be synthesized with a wet chemistry protocol. Size, shape, and composition can be well controlled. As that is beyond the focus of this article, we will only briefly introduce it here.

Synthesis of bimetallic nanoparticles can be categorized into (1) co-reduction (or co-decomposition) of two precursors, (2) two-step reduction (or decomposition) of metallic precursors, (3) electrochemical reduction of metallic precursors, and (4) reduction of a double complex, and other methods.

In the first method, two precursors are mixed in a solvent, typically an alcohol. Both of the two precursors are reduced or decomposed in a pot and form bimetallic nanoparticles. A polymer such as PVP is frequently used as a surface stabilizer. In many cases, bimetallic nanoparticles of two noble metals can be synthesized with this protocol. However, the protocol could be quite different if one of the metals is a 3d metal such as Cu, Ni, Co, *etc*. This is because the light transition metals have lower redox potentials of the corresponding metal ions in contrast to those of the noble metal ions and they can be oxidized readily. To synthesize a bimetallic nanoparticle consisting of a noble metal (Pt, Pd, Rh) and a light transition metal, a glycol solvent such as ethylene glycol with a high boiling point is necessary for refluxing the precursor at a high temperature. In many cases, glycol acts as a reducing agent as well.

In terms of the two-step reduction process, it is typically used for the synthesis of bimetallic core–shell nanoparticles. Basically, it requires the deposition of one metal element (***B***) on pre-synthesized monometallic nanoparticles of another metal (***A***), called seeds in some cases. However, if the difference in redox potentials of the two metals is small, they could form *metal A-rich* core *@metal B-rich* shell structured bimetallic nanoparticles instead of a nanoparticle consisting of a *pure metal* ***A*** *core* and a *pure metal* ***B*** *shell*. This is because metal ions of metal ***B*** could oxidize metal atom ***A*** ($\boldsymbol{A^0}$) of the core to produce metal atom ***B*** ($\boldsymbol{B^0}$) and metal ion A^{n+}. Then, metal atoms ***B*** will deposit on nanoparticles of metal ***A*** (Fig. 1b2). The newly formed A^{n+} in the solution will be reduced to form metal atom ***A*** and deposit on the atomic layer B (Fig. 1b3). In addition, different amounts of metal ions A^{n+} could be 're-reduced to metal atoms ***A*** ($\boldsymbol{A^0}$) by reducing agent during the reduction of metal ions B^{m+} into metal atoms B^0. To some extent, metals A and B form an alloy in the shell of the nanoparticles. Fig. 1b schematically shows the process of a successive reduction in the synthesis of bimetallic nanoparticles with wet chemistry.

Different from the reduction of metal ions using a reducing agent, electrochemical reduction can form metal atoms from bulk materials directly at room temperature.[35,36] Typically, a bimetallic bulk material ($A_{1-x}B_x$) is used as an anode and Pt is used as a cathode. It includes two processes: oxidation of the anode to generate two types of metal ions, and then reduction by electrons produced from the Pt cathode through reduction. Surface surfactant is added to an electrochemical cell to prevent the formed metal atoms from aggregation in the electrolyte during the formation of a bimetallic nanoparticle.

Reduction of a double complex is another method to synthesize bimetallic nanoparticles.[36,37] The two metal ions in a double complex are reduced simultaneously. The size of the formed bimetallic nanoparticles is determined by the concentration of the double complex. A challenge in the use

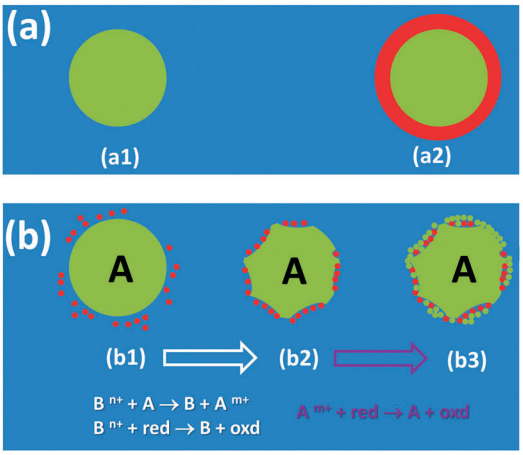

Fig. 1 Two typical approaches to the synthesis of bimetallic nanoparticles.

of this method is the availability of a double complex. Only a limited number of double complexes are available.

Other than these wet chemistry methods, dry chemistry, mostly an e-beam evaporation followed by a vacuum deposition on a substrate can form bimetallic nanoclusters on the support. In most cases, two sources of metals ***A*** and ***B*** are evaporated simultaneously or successively to form bimetallic nanoclusters with different compositions and structures. Alternatively, metal ***A*** can be deposited on a substrate of the oxide of metal ***B***. A subsequent reduction will form a bimetallic catalyst. As this method does not use any organic solvent or surfactant, the surfaces of bimetallic nanoparticles prepared with this method are clean. One advantage is that these methods can be used to grow bimetallic nanoclusters on any substrates,[38] which offers the opportunity of studying the effects of support materials in catalysis. Another advantage of dry chemistry preparation is the universal feasibility of the preparation of any bimetallic nanoclusters since the growth kinetics are much more straightforward without a strong dependence on the types of metals.

3. Techniques to study restructuring

Catalysis, essentially a surface property of catalytic materials, results from one to several atomic layers on or below a surface. Most heterogeneous catalytic reactions are performed on catalyst surfaces at a temperature higher than room temperature at solid–gas or solid–liquid interfaces in gaseous or liquid environments, respectively. Due to the high surface free energy, under-coordinated chemical environments of surface atoms, thermal diffusion of atoms in the surface region, and binding of reactant molecules and/or dissociated species, the surface structure of a catalyst is highly dynamic.[19] Typically, an entity of one or more under-coordinated surface atoms are active for catalysis. It is critical but challenging to identify the authentic surface chemistry and structure under reaction conditions during catalysis (phase B in Fig. 2) due to technical barriers.

3.1 Ambient pressure techniques studying surface chemistry of catalysts

To study the surface chemistry of catalysts at near ambient pressure conditions, vibrational spectroscopies can track

Possibility	Before catalysis (as-synthesized or as-pretreated)	During catalysis (active phase)	After catalysis	Operando Studies
#1	Phase A	Phase A	Phase A	
#2	Phase A	Phase B	Phase B	
#3	Phase A	Phase B	Phase A	√
#4	Phase A	Phase B	Phase C	√

Fig. 2 Evolution of phase of a heterogeneous catalyst before catalysis, during catalysis, and after catalysis.

vibrational signatures of adsorbates and sometimes substrates such as some oxide catalysts. *In situ* and operando studies of surface structure and chemistry of *catalysts* (surface coordination, oxidation state, atomic arrangement) have been an under-represented component in operando studies until recent years. Synchrotron-based ambient pressure XPS (AP-XPS) technique invented by Berkeley scientists in 2002 has made the study of surfaces at a near ambient pressure conditions possible.[17,39] The feature of this AP-XPS is the use of focusing lenses which increase the collection rate of photoelectrons escaping from an aperture. The aperture is used to separate the near ambient pressure reaction environment and vacuum environment. The distance between the surface of a sample and aperture is in the range of the mean free path of photoelectrons in the Torr pressure range. Later on, a new synchrotron-based ambient pressure XPS was installed on beam 9.3.2 by Liu and co-workers.[40] So far the AP-XPS technique has been available in a few synchrotron centers around the world. It is has been one of the main techniques characterizing surface chemistry (surface composition, oxidation state, and electronic state) of catalysts under reaction conditions and during catalysis.

Fig. 3 schematically shows an AP-XPS system invented in 2002.[39] An important idea implemented in ambient pressure XPS technique[39] is the short distance between a sample surface and the small aperture which separates the ambient environment of the catalysts and the vacuum environment of the energy analyzer. The distance is approximately kept at the length of the mean free path of photoelectrons in gases with certain pressure. For example, it is about a couple of mm for

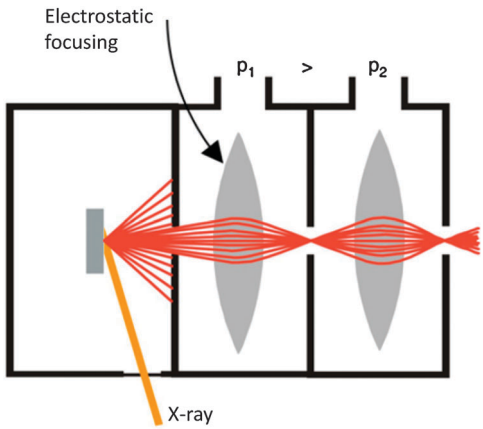

Fig. 3 Schematic of ambient pressure X-ray photoelectron spectroscopy (AP-XPS). (Reproduced from ref. 17.)

photoelectrons of 400 eV in 1 Torr of nitrogen.[17] Upon escaping from the gas environment between a sample surface and an aperture, the photoelectrons will travel in the pre-lens vacuum ($\sim 10^{-4}$ Torr). Focusing lenses are installed at the differential pumping stages which increase the collection rate of photoelectrons before entering the energy analyzer.[15,39,41]

3.2 Ambient pressure analytical techniques studying surface structures of catalysts

A single event of heterogeneous catalysis is performed on a catalytic site consisting of one, two, or more atoms. These sites could have different atomic arrangements and electronic states. The surface of a catalyst particle, typical the smallest crystallite with a size of 1–100 nm could be quite heterogeneous since the fraction of atoms at corners and edges is not negligible at the nanoscale. This fraction is increased with a decrease in the size of catalyst crystallites. Notably, atoms at a corner or on the edges have a lower coordination number than atoms on the terrace. Typically, atoms at step edges have a larger adsorption energy in contrast to atoms on a terrace. Thus, many reactant molecules are preferentially adsorbed on an edge or corner or other defect sites. More importantly, the surface structure of these under-coordinated sites could experience significant changes at the high temperatures of catalysts in high pressures of reactants in contrast to that as-synthesized. In terms of the temperature factor, the increased mobility largely increases the opportunity of rearrangement of atoms on surfaces. Temperature has much larger impact on under-coordinated atoms compared to atoms on a terrace.[42] Pressure of reactants is another factor; the increased contribution of entropy at higher pressure could potentially change the ΔG of a surface and thus restructure the surface at a high pressure. In addition, one factor playing an important role in restructuring is the reaction between surface atoms of a catalyst and reactant molecules or dissociated species. Such a reaction could change surface structure or form a completely new phase under reaction conditions. Thus, surface structure at the atomic level under reaction conditions or during catalysis is a critical parameter in understanding catalysis toward the design of new catalysts.

Surface structure of bimetallic model catalysts such as bimetallic nanoclusters prepared by e-beam evaporation and deposition can be visualized with STM under reaction conditions or during catalysis. In many cases, STM is used to study surface structure at low temperatures in UHV. In these applications, the tunneling junction is under an ultrahigh vacuum environment. Electrons are directly tunneled through the vacuum junction. As the tunneling junction is in the range of a few angstroms, the existence of a couple or a few layers of floating molecules (randomly distributed) does not weaken the capability of identification of surface structure at an atom scale.

Development of STM instrumentation with the goal of bridging the pressure gap has been done in several groups.[43–46] Many of them implemented the strategy of filling gases into chambers with different sizes.[19,47,48] Recently, an ambient pressure high temperature STM (APHT-STM) with a flowing cell has became available.[49] This APHT-STM has the capability of visualizing surface structures at a temperature of 300 °C in a gaseous environment up to 50 Torr.

X-Ray absorption and the related techniques are important techniques used to explore bimetallic catalysts during catalysis under reaction conditions. One of their unique functions is to identify coordination number and oxidation state of metal atoms of a catalyst. They have been developed in the past two decades.[50,51] A review of applications of this technique to the studies of bimetallic nanoparticles will be given elsewhere in this themed issue. Thus, the principle of this application will not be repeated here.

Other than these techniques briefly described above, environmental TEM (ETEM) has been one of the most powerful techniques for studying structures and compositions of catalysts under reaction conditions or during catalysis.[22,52–56]

4. Restructuring under reaction conditions at solid–gas interfaces

Segregation of atoms of element ***A*** from bimetallic catalysts A_xB_{1-x} was demonstrated early in the vacuum surface sciences and catalysis.[57–59] The driving forces from the point of view of thermodynamics are the different surface energies of the two metals (***A*** and ***B***) and/or the different adsorption energies of molecules on atoms of the two metals. In a UHV environment, the surface energy of atoms is the only driving force if there is no adsorbate. In most cases, the segregation is not kinetically favorable at room temperature; thus annealing bimetallic materials to high temperature can accelerate the segregation, forming a surface layer with a quite different composition in contrast to deep layers of this bimetallic material. Thus, annealing in UHV could promote the segregation of atoms of a metal with low surface energy from deep layers to the surface. The surface composition after annealing is different than that before annealing. This is actually the segregation of bimetallic catalysts without adsorption in UHV. However, recent studies showed the compositions at both a surface region and the "bulk" of these bimetallic materials are quite different from those before annealing if the metal is on the nanoscale. A massive segregation in bimetallic nanoparticles.

In the vacuum surface science approach, typically reactant molecules are introduced to the surface of a bimetallic material (a bulk single crystal or nanoparticle) by exposing the surface to certain pressures of the reactant gases such as CO or H_2 (typically lower than 10^{-7} Torr) for a certain amount of time. Typically, the experiments are performed at room temperature. Thus, a chemisorbed layer of reactant molecules is formed on the surface of a bimetallic catalyst. After a certain amount of time, the reactant gas is purged to restore the UHV environment necessary for UHV-based surface analytical techniques such as vacuum XPS. As the reactant gas only forms a static sub-monolayer or a monolayer of adsorbates on the surface, the factor of adsorption energy could not play a major role in the restructuring. Thus, the segregation or restructuring of bimetallic catalysts in UHV is mainly driven by the factor of the surface energy of the two elements even though a layer of adsorbates is formed.

In the case of bimetallic catalysts under reaction conditions or during catalysis the segregation of bimetallic nanoparticles

is much more vigorous. It is typically called *restructuring* of bimetallic nanoparticles instead of *segregation*. Certainly, the different surface free energy of the two metals is one of the factors. However, the continuous supply of reactant molecules in an environment of reactant gases at a relatively high pressure and the large mobility of atoms at a relatively high temperature typically make the restructuring extensive.[5,7] The high temperature of catalysts provides sufficient energy to atoms of the subsurface to migrate to the topmost surface layer through a thermal diffusion. If the reactant molecules preferentially bind to atoms of metal A or B, the atoms (A or B) with the higher binding energy in the topmost surface layer will segregate to the surface. For a bulk crystal of a bimetallic catalyst, the migration of metal atoms from subsurface or deeper layer to the topmost layer is challenging. In this case, a high temperature is required. As the source of adsorbates is infinite during catalysis and thermal diffusion at high temperature is enhanced, the segregation of atoms to the surface under reaction conditions or during catalysis is continuous.

For bimetallic nanoparticles with size at nanometres, the fraction of under-coordinated metal atoms including atoms at a corner or on a step edge is much larger than that of a bulk bimetallic catalyst. These under-coordinated atoms typically experience a high mobility. Thus, the subsurface atoms of bimetallic nanoparticles can segregate to the surface through the atoms at corners or edges even though reactant molecules have bound to these low-coordinated atoms. Thus, with a relatively low diffusion barrier the surface metal atoms in deeper layers can continuously segregate. For example, atoms of element ***A*** continuously segregate to the surface and immediately bond with the reactant molecules. Notably, thermal diffusion at high temperature will allow fresh atoms of deep layers to segregate to the surface. Then, these metal atoms in the surface layer will chemisorb molecules or intermediates. As the segregation is a continuous process during catalysis or under reaction conditions, the surface layer with bonded adsorbates (such as oxide) will be replaced by fresh atoms of deeper layers. Eventually, a new thick surface region consisting of atoms of element ***A*** binding to the reactant molecules will be formed. This process forms an element ***A***-rich surface region and an element-***B*** rich core region. This restructuring is more dramatic in contrast to the segregation of bimetallic catalysts in UHV since the segregation under reaction conditions is typically a continuous process. We term it massive restructuring of bimetallic nanocatalysts under reaction conditions or during catalysis.

4.1 Rh–Pd

The restructuring of rhodium and palladium bimetallic nanoparticles under reaction conditions was studied using AP-XPS.[5,7] $Rh_{0.5}Pd_{0.5}$ bimetallic nanoparticles with diameters of 15 ± 1 nm were synthesized with a colloidal chemistry method and deposited on a silica layer of a silicon wafer. Depth-profile analysis using X-ray energies of 1486.6 eV (Al Kα), 850 eV, and 645 eV corresponding to inelastic mean free paths (IMFP) of approximately 1.6, 1.0, and 0.7 nm for photoelectrons of Rh3d and Pd3d, respectively, were performed. A Rh-rich shell and Pd-rich core were identified. In the surface region of $\sim$0.7 nm, the atomic fraction of Rh is 97% (Fig. 4a).

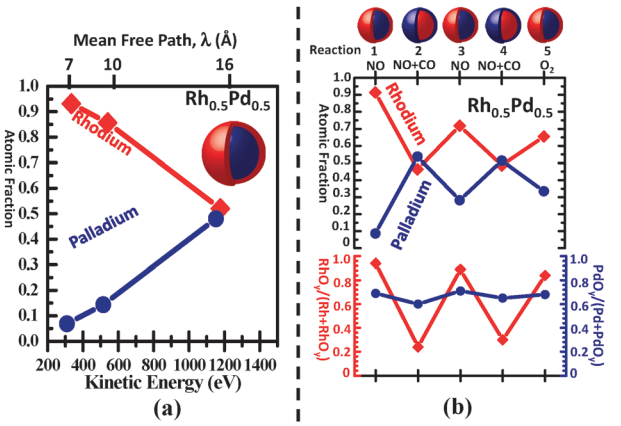

Fig. 4 (a) Surface structure of as-synthesized $Rh_{0.5}Pd_{0.5}$ and (b) evolution of atomic fractions of rhodium and palladium in the surface region (upper panel) and fraction of oxide in the total amount of metal and oxide (lower panel) (λ = $\sim$0.7–1.0 nm) under different reaction conditions (reducing gases or oxidizing gases at 300 °C). XPS spectra were collected when the reactant gases were present and reactions were going on. (Reproduced from ref. 5.)

The surface composition and chemical state of $Rh_{0.5}Pd_{0.5}$ bimetallic nanoparticles were investigated under oxidizing (100 mtorr NO or O_2), catalytic (100 mtorr NO and 100 mtorr CO), and reducing (100 mtorr CO or H_2) conditions using a synchrotron-based AP-XPS. The surface composition obtained with an X-ray energy of 645 eV, which corresponds to a 0.7 nm IMFP of Rh 3d and Pd 3d, represents the composition and chemical state changes in the shell region. Fig. 4b presents the atomic fractions of Rh and Pd of the $Rh_{0.5}Pd_{0.5}$ bimetallic nanoparticles under different reaction conditions. There is no obvious difference in surface composition of Rh and Pd between particles in oxidation conditions and those of the as-synthesized. This is because the reflux at 220 °C in the solvent PVP during synthesis followed by exposure to the ambient environment made the surface region of the bimetallic nanoparticles oxidized. A notable change in surface composition upon switching the reaction conditions to reducing environments (H_2 or CO at 300 °C) was revealed using AP-XPS (Fig. 4b). In this restructuring, the atomic fraction of Rh in the shell region decreased to 46% and Rh reduced to metallic atoms (lower panel of Fig. 4b). Palladium actually experienced the opposite change. The atomic fraction of Pd increased in oxidizing gases. It shows Pd atoms segregate to the surface region. The change in the surface composition of the bimetallic nanoparticles and the reducing of metal oxide and oxidation of metal resulting from changing of reactant gases is called reaction-driven restructuring of bimetallic nanoparticles.[5,18,26,27,60]

When the reactant is changed to NO, the atomic fraction of rhodium in the surface region increased by 40%. The significant increase in the atomic fraction of rhodium in the surface region clearly shows that the restructuring is performed in a surface region thicker than the sampling depth. A following study of the restructuring behavior of Rh–Pd bimetallic foil[61,62] shows a restructuring to a lesser extent compared to $Rh_{0.5}Pd_{0.5}$ bimetallic NPs. The difference in restructuring behavior between bimetallic nanocatalysts and bimetallic foil suggests a difference in the

depth of restructuring. As the fraction of atoms at edges and corners of nanoparticles is much larger than that in foil, under-coordinated atoms at corners and edges accelerate the segregation of atoms from deeper layers and migration of metal atoms in top surface layers to deep layers. A similar difference in the behavior of restructuring was revealed in Pd–Au nanoparticles[4] and Pd–Au single crystals.[16,63–65]

4.2 Rh–Pt

Rh–Pt are important catalysts in environmental remediation and energy conversion.[1] Similar to the investigation of Rh_xPd_{1-x} bimetallic nanoparticles, XPS depth profile studies using X-ray energies of 645, 850, and 1486.6 eV for Rh 3d and 350, 600, and 1486.6 eV for Pt 4f were performed.[7] The depth dependence of the atomic percentage of Rh and Pt in the Rh_xPt_{1-x} bimetallic nanoparticles is much weaker than that in the Rh_xPd_{1-x} case, indicating that the Rh_xPt_{1-x} bimetallic nanoparticles are intermetallic instead of a core–shell structure. The restructuring process in the surface region of Rh_xPt_{1-x} bimetallic nanoparticles under reaction conditions was studied in oxidizing (NO) or reducing (CO or H_2) conditions at 300 °C using AP-XPS (Fig. 5a). Rh_xPt_{1-x} bimetallic nanoparticles were restructured (even if they are an alloy instead of core–shell structures) when switching the surrounding reactant gas between reducing and oxidizing gases. Rh segregates to the surface of nanoparticles and is oxidized under the oxidizing conditions at 300 °C.

The restructuring of Rh_xPt_{1-x} can be rationalized by two factors: adsorption energy of molecules or dissociated species and surface energy of metal atoms. In a reducing environment such as H_2, Pt has a low surface energy compared to Rh; thus Pt preferentially segregates to the surface. However, in an oxidizing environment, the adsorption energy of oxygen atoms on Rh is actually larger than that on Pt; thus surface Rh can be preferentially oxidized and even Rh atoms in deep layers continuously segregate to the surface and are then oxidized. The Rh metal in the surface region is continuously replaced with the formed RhO_x thus a thick RhO_x surface shell is formed.

The understanding of the driving force for surface restructuring of bimetallic nanoparticle catalysts under reaction conditions is of great value for predicting the surface structure of bimetallic catalysts under reaction conditions during catalysis.

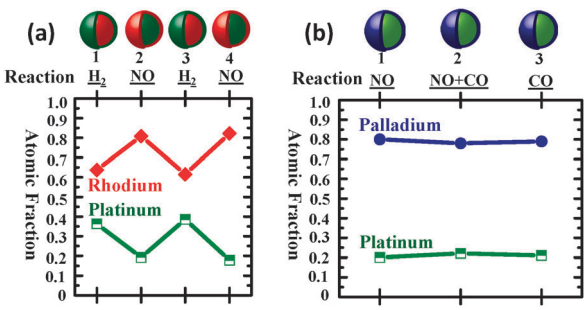

Fig. 5 Evolution of atomic fractions of constituent elements in the surface region (λ = ~0.7–1.0 nm) under different reaction conditions (reducing gases or oxidizing gases at 300 °C). XPS spectra were collected when the reactant gases were present and reactions were going on. (a) $Rh_{0.5}Pt_{0.5}$, (b) $Pt_{0.5}Pd_{0.5}$. (Reproduced from ref. 7.)

In fact, the above two factors can also rationalize the absence of change in the surface composition of $Pd_{0.5}Pt_{0.5}$ bimetallic nanoparticles (Fig. 5b) even though the oxidation state of Pd is changed in oxidizing environments compared to reducing ones. Under a reducing environment of CO or CO + NO, both Pd and Pt exist in a metallic state. Pd and Pt have a similar adsorption energy for CO. However, Pd has a low surface energy in contrast to Pt. Thus, Pd preferentially segregates to the surface. In the reactant NO, NO dissociates into nitrogen or oxygen atoms. As the binding energy of oxygen atoms on Pd atoms is larger than that on Pt, Pd preferentially remains in the surface region in the format of PdO_x in oxidizing environments. Overall, atomic fractions of Pd and Pt do not change when the reactant gas is changed from CO or H_2 to NO or O_2. But their oxidation state is changed alternatively.

4.3 Pd–Ag

A fundamental study of surface composition and oxidation state of Pd–Ag is critical since Pd–Ag and other Pd-based bimetallics are important catalysts in the hydrogenation of unsaturated hydrocarbons.[1] Kitchin *et al.* used an *ab initio* atomistic thermodynamic approach to study the Ag_3Pd alloy in an O_2 environment.[66] The surface free energy of Ag-rich or Pd-rich $Ag_3Pd(111)$ in equilibrium with oxygen as a function of the oxygen chemical potential was calculated (Fig. 6). In UHV conditions more Ag is present on the surface in contrast to that in the bulk, resulting from a low surface free energy of Ag.

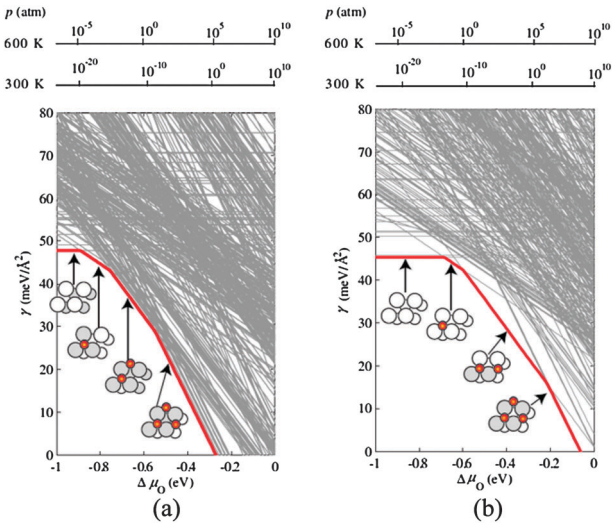

Fig. 6 Surface free energy of $Ag_3Pd(111)$ in equilibrium with a Pd-rich Ag_3Pd bulk reservoir (a) and Ag-rich Ag_3Pd bulk reservoir (b) as a function of oxygen chemical potential. Each line corresponds to one of the tested surface configurations, and only the few configurations that result as most stable for a range of oxygen chemical potentials are drawn as dark (red) lines. Additionally shown as insets are top views of the most stable surface configurations with adsorbed O atoms shown as small (red) circles, Ag atoms as white circles, and Pd atoms as grey circles. The dependence on the oxygen chemical potential is translated into pressure scales using: $\mu_{O_2}(\mathrm{gas})(T, p_{O_2}) = E_{O_2}(\mathrm{gas})^{\mathrm{total}} + 2\Delta\mu_o(T, p_o) + k_B T \ln\left(\frac{p_{O_2}}{p_o}\right)$ for T = 300 K and T = 600 K (upper x axes).[66] (From ref. 66.)

There is a competition *between* the segregation of metal atoms with a lower surface free energy to decrease the total surface free energy *and* the pinning of atoms which bind to reactant molecules or dissociated species strongly. As the chemical potential of oxygen is increased, the adsorption energy of oxygen atoms plays an important role. The two opposite factors compete here. The calculation showed that the adsorption of oxygen drives the segregation of Pd to the surfaces, increasing the Pd concentration in the first two layers.

As Pd–Ag is an active catalyst in the hydrogenation of unsaturated hydrocarbons, fundamental studies of surface restructuring of Pd–Ag in H_2 is important. Pd–Ag bimetallic catalysts exhibit surface segregation in H_2. Pd surface segregation is performed on the high hydrogen pressure side of a PdAg membrane.[67] Neyman *et al.* theoretically studied the surface structure of a $Pd_{0.8}Ag_{0.2}$ alloy and predicted its modification in the presence of atomic hydrogen.[68] In the absence of adsorbates in UHV, the surface is predicted to expose mostly silver atoms, due to the low surface free energy of Ag. In the presence of H_2, Pd progressively separated to the surface and thus restructured. With the increase of surface coverage of hydrogen, the termination of Pd atoms with hydrogen atoms compensated for the energy gain resulting from the presence of Ag atoms on the surface due to its low surface energy. Thus, surface segregation of Ag atoms was largely prevented in the environment of H_2. Notably, as Ag atoms are located at the sub-surface, the propensity of H atoms to accommodate interstitial sites of Pd below the surface vanishes. Thus, in the environment of hydrogen, Pd atoms are preferentially exposed in the topmost surface layer of Pd–Ag bimetallic catalysts.

4.4 Pd–Au

Pd–Au is active for many catalytic reactions such as CO oxidation and synthesis of vinyl acetate.[16] Restructuring of the Pd_xAu_{1-x} bimetallic nanoparticle system during CO oxidation was studied using AP-XPS.[4] Both STEM/EDS phase mapping of single nanoparticles and XPS depth profiles indicate that the as-synthesized Pd_xAu_{1-x} (x = 0.25, 0.5, 0.75) bimetallic nanoparticles have core–shell structures with Pd-rich shells and Au-rich cores. With the increase in Au percentage, the Au core size increases while the thickness of the Pd shell decreases. AP-XPS studies show that the surface compositions and oxidation states of $Pd_{0.75}Au_{0.25}$ and $Pd_{0.5}Au_{0.5}$ nanoparticles at 200 °C in CO oxidation are similar to that in vacuum (Fig. 7a and b).

For $Pd_{0.25}Au_{0.75}$ nanoparticles in CO oxidation, the factor of surface energy plays a major role. The lower surface energy of Au results in a Au-rich surface. This restructuring is irreversible due to more energy gained from segregation of Au atoms from deep layers since the overall fraction of Au in a single NP is high. Although the adsorption of CO on Pd can decrease surface energy, the gained energy through adsorption is not enough to compensate for the decreased energy in segregation of Au due to a low adsorption energy of CO on Pd atoms coordinating with Au in Au-rich surface in contrast to CO on a Pd atom coordinating with all Pd atoms.

The catalytic studies of those Pd_xAu_{1-x} bimetallic nanoparticles for CO/O_2 reactions show a 'synergistic effect' for the

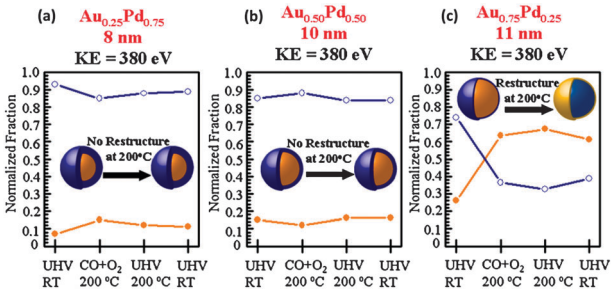

Fig. 7 Atomic fractions of gold and palladium in the surface region of $Au_{0.25}Pd_{0.75}$ (a), $Au_{0.5}Pd_{0.5}$ (b) and $Au_{0.75}Pd_{0.25}$ (c) under different reaction conditions. The atomic fractions were measured with AP-XPS which sampled photoelectrons from Au 4f and Pd 3d levels with a kinetic energy of 380 eV.[4] (From ref. 4.)

plots of turnover rates *versus* the surface composition. All bimetallic nanoparticles have higher turnover rates than monometallic Au or Pd nanoparticles. Notably, the Pd-deficient surface ($Pd_{0.25}Au_{0.75}$) exhibits a relatively low TOF; it probably results from low binding energy of CO since the Au atoms have an electron density that is more extended.[69,70] Another reason could be the absence of a Pd pair site for O_2 dissociation on a Pd-deficient surface.

In contrast to Pd_xAu_{1-x} nanoparticles, the surface chemistry of Au–Pd bimetallic catalysts in CO oxidation was studied on a AuPd(100) single crystal.[71–76] Different than Pd_xAu_{1-x} bimetallic nanoparticles dispersed on silica, there is no support for AuPd(100) single crystals. The low fraction of Pd in the top surface layer is not active for CO oxidation. However, the high pressure of reactants promotes the segregation of Pd to the surface. This is related to the high coverage of CO and O at high pressure. The segregation of Pd on AuPd(100) is dependent on the coverage of oxygen atoms. A minimum coverage of 1/3 is necessary to initialize the surface segregation of Pd. Interestingly, once segregated to the surface, Pd atoms do not have the tendency to form clusters due to weak interactions.[77]

Catalysis studies showed there is a correlation between the presence of contiguous Pd sites (a pair of Pd monomers) and the reactivity. The formed continuous Pd sites respond for O_2 dissociation. Both Au and Pd atoms on the AuPd(100) surface can adsorb CO molecules. However, the adsorption energy on AuPd(100) is lower than that on a monometallic Pd surface. Sites of Pd atoms in the topmost surface are more active for CO oxidation with a low activation energy in contrast to a pure Pd catalyst. One of the reasons is the lower binding energy of CO on Pd atoms which minimizes the CO inhibition.

In contrast to the restructuring of Pd–Au bimetallic single crystal model catalysts, the amount of segregated Au or Pd of Au_xPd_{1-x} bimetallic nanoparticles is larger.[4] A low pressure of 0.1 Torr of reactant gas can restructure the surface of bimetallic nanoparticles significantly.[4] This is consistent with the difference in segregation between Rh_xPd_{1-x} bimetallic nanocatalysts[5,7] and Rh_xPd_{1-x} bimetallic film[78] reviewed in section 4.1. For a metal *nanoparticle*, there is a large fraction of metal atoms with lower coordination numbers at the corners or on the edges in contrast to that of metal crystals or thin films. The under-coordinated Pd atoms in the topmost surface of bimetallic NPs provide the "special" sites of restructuring.

These special sites make the segregation significant due to a low segregation barrier at these sites.

4.5 Pd–Cu

Segregation of $Pd_{0.5}Cu_{0.5}$(110) single crystal in UHV was studied[79] using a medium-energy ion scattering, a surface analytical technique with the unique ability to provide information on surface composition with depth resolution at the level of atomic layer for crystalline materials. Adsorption of hydrocarbons or hydrogen induces Pd segregation in Pd catalysts significantly when alloyed with elements like Cu, Ag or Au. In fact, for a molecule with strong electronegative functional groups such as trichloroethene, a reverse segregation could occur. For example, upon adsorption of trichloroethene, Cu is segregated and the first three layers become rich in Cu due to the relatively electropositive 3d metal compared to Pd.[79]

A similar behavior of restructuring was observed on Pd_xCu_{1-x} nanoparticles supported on zeolite. The structure and chemistry of Pd_xCu_{1-x} bimetallic nanoparticles were explored by using XANES and FTIR under reaction conditions of CO hydrogenation.[80] The alloy phase of Pd_xCu_{1-x} nanoparticles formed under the reaction conditions is in fact disordered. FTIR studies suggest the adsorption of CO and H_2 induces a segregation of Pd atoms to the surface under high pressure reaction conditions. Meanwhile, the formation and deposition of copper carbonyl during CO hydrogenation were revealed by FTIR. Although Pd continuously segregates to the surface in CO, the fraction of Pd with three-fold sites actually decreases as a function of time in the mixture of H_2 and CO.

4.6 Pd–Zn

In the middle of the 1990s, Pd supported on ZnO was demonstrated as a potential catalyst to generate H_2 from methanol without or with a limited amount of CO produced.[81,82] The ZnO supported Pd turns the methanol steam reforming to the production of CO_2 and H_2 instead of a direct decomposition into CO and H_2 on Pd supported on an inert support such as silica. An active phase of Pd alloying Zn was suggested on the basis of its catalytic behavior.[82] X-Ray absorption spectroscopy confirmed the formation of Pd–Zn alloy during catalysis.[83] The on-line measurement of catalytic performance suggested that the Pd–Zn alloy is the active phase for methanol steam reforming.[14,83] *In situ* AP-XPS studies confirmed that the active phase is the Pd–Zn alloy (Fig. 8) formed under the reaction conditions of methanol steam reforming.[15,84] The formation of Pd–Zn intermetallics during catalysis was identified. It results from the reduction of ZnO by hydrogen under the reaction conditions since H_2 is the major product. The hydrogen was produced in the early step of methanol decomposition on Pd. Hydrogen atoms spillover to ZnO and thus reduce ZnO to metal Zn which alloys with Pd atoms to form Pd–Zn intermetallics (Fig. 8c).

Notably, the Pd–Zn alloy de-alloys in an environment of oxygen. The formation and dealloying of Pd–Zn bimetallics are reversible in reducing and oxidizing environments, respectively. In addition, *in situ* studies showed the thickness of the Pd–Zn alloy increases with the reduction time. Interestingly, the thick PdZn intermetallic exhibited high selectivity for the production of CO_2 in contrast to the monolayer Pd–Zn layer which is active for the

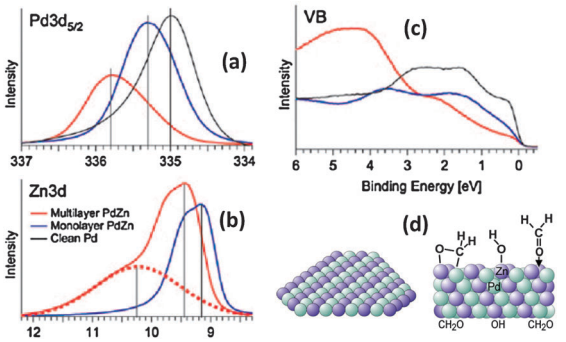

Fig. 8 Photoemission features of PdZn catalyst studies with ambient pressure photoelectron spectroscopy taken during methanol steam reforming on the PdZn 1 : 1 multilayer (red curves) and monolayer alloy (blue curves). (a) Pd 3d, (b) Zn 3d, and (c) valence-band (VB). (d) Left panel p(2 × 1) surface structure of the 1 : 1 multilayer PdZn alloy on Pd(1 1 1). Right panel: side view of the multilayer PdZn alloy with likely surface intermediates reacting toward CO_2.[15] (From ref. 15.)

production of CO and H_2 though they have identical atomic fractions. This is illustrated in Fig. 8d.[14] This difference suggests the electronic density of a monolayer of Pd–Zn formed on Pd is quite different than that of thick Pd–Zn alloy.

4.7 Ag–Cu

Ag is an important catalyst for epoxidation of ethylene. This reaction could produce ethylene oxide which is the ideal product, along with the thermodynamically favorable by-product acetaldehyde. Alloying Ag with a small atomic fraction of Cu improves the selectivity to ethylene oxide significantly.[85–87] First principle computation[88–90] and ambient pressure XPS studies[88] revealed that the surface composition and chemistry of the Ag–Cu catalysts are in a state of non-equilibrium during catalysis. Thus, the authentic composition is dependent on the specific reaction conditions. Fig. 9 is the calculated surface phase diagram of Ag–Cu in the mixture of O_2 and C_2H_4.[88] The predicted surface phase was confirmed experimentally.[88]

In an oxygen environment, Cu segregates to the topmost layers due to the stronger Cu–O bond in contrast to Ag–O (top-right in Fig. 9). Thus, a thin copper oxide layer is formed. Coexistence of a thin copper oxide layer at the surface of the alloy was suggested in the mixture of C_2H_4 and O_2 under reaction conditions. The observation of oxidized Cu suggested the enhanced catalytic selectivity results from the involvement of oxygen atoms of CuO formed on the surface during the catalysis.

4.8 Ag–Au

Ag–Au alloy nanoparticles supported on mesoporous silicate show exceptionally high activity on CO oxidation which was comparable to the most active catalyst, Au–TiO_2. The solution of Au–Ag bimetallic nanoparticles was mixed with a sodium aluminosilicate solution and followed with a hydrothermal reaction. No detection of metallic Ag on the Ag@MCM shows that the calcination leads to a complete conversion of metallic Ag to AgBr. For the Ag–Au bimetallic nanoparticles, complete phase segregation occurred during calcination, resulting in the formation of Au and AgBr. This is confirmed

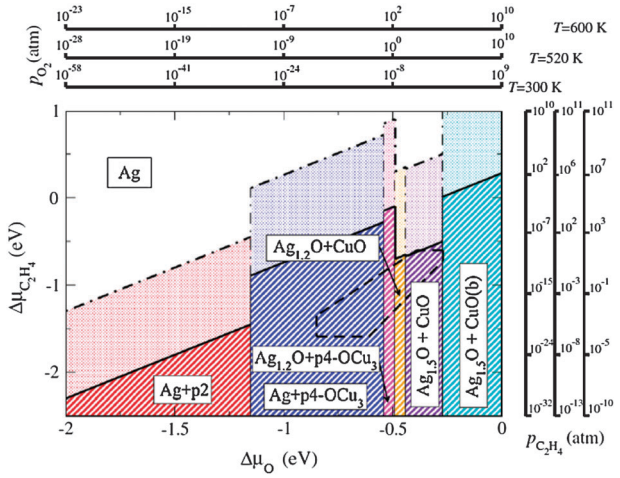

Fig. 9 Surface phase diagram for the (111) facet under constrained thermodynamic equilibrium with oxygen and ethylene. Solid (dot-dashed) lines represent the stability limit with respect to the formation of CH_3CHO (C_2H_4O). Each shaded area represents the region of stability of a combination of two surface structures giving a Cu coverage of 0.5 ML. The white area is the region of stability of the clean Ag(111) surface. The dashed polygon corresponds to typical values of temperature and pressures used in experiments (T = 300–600 K and pO_2, pC_2H_4 = 10^{-4} to 1 atm). $Ag_{1.2}O$ and $Ag_{1.5}O$ are 1-layer thin oxide-like structures; CuO and CuO(b) are 1-layer thin and bulk CuO structures, respectively; p2 and p4-OCu_3 are 1-layer thin Cu_2O-like structures with (2 × 2) and (4 × 4) periodicity, respectively. In the latter, an OCu_3 unit is removed.[88] (From ref. 88.)

by the chemical state of Ag in the calcined samples (+1), while Au remains in metallic form. The surface concentration of Au and Ag from XPS results shows the calcined sample has a Ag-rich surface. Au L3 edge EXAFS spectra of all Au–Ag/MCM catalyst shows the same feature as pure Au@MCM, indicating the nearest neighboring atom is Au instead of Ag. It is clear that the Au–Ag alloy nanoparticles restructured into a Au@AgBr structure upon calcination. These calcined samples of Au–AgBr did not exhibit any catalytic activity for CO oxidation as expected. A subsequent high temperature hydrogen reducing pretreatment up to 700 °C leads to high catalytic activity in CO oxidation. Catalysts that experienced a reduction treatment between 550 and 600 °C have the highest activity in CO oxidation. XPS studies of catalysts after reduction confirmed the reduction of Ag^+ to metallic Ag and the removal of Br^- ions. The EXAFS studies confirmed that the restructuring was performed during reduction with H_2. Both Au L3 edge and Ag K edge EXAFS spectra of reduced samples varied with different Au–Ag ratios, indicating the formation Au–Ag alloy.

4.9 Au–Cu

The chemistry and structure of AuCu bimetallic nanoparticles supported on SBA-15 were studied using multiple *in situ* techniques (XRD, FT-IR, XANES).[91] Au–Cu catalysts are highly active in CO oxidation below room temperature. An as-prepared Au–Cu nanoparticle is made up of a gold core decorated with CuO patches.[91] During the activation in a reducing gas, the CuO patches away from the interface between the catalyst particles and SBA-15 support were reduced to metallic Cu and migrated into the core. In fact, an intermetallic phase Au_3Cu_1 was formed during this pretreatment. The CuO at the interface was reduced to a Cu_2O phase acting as a "nanosticky" between the metallic phase and the surface of the SBA-15 support. The Cu_2O stabilizes the metallic particles, which explains the absence of aggregation of metal nanoparticles at a high temperature. This actually also rationalizes the preservation of size of Rh–Pd and Au–Pd bimetallic nanoparticles supported on silica even at 300 °C after a reaction at 300 °C in Torr pressure of H_2 or CO for several hours.[4,5]

Interestingly, during CO oxidation, Cu segregated to the surface and was oxidized into CuO_x patches. This restructuring resulted in metal-oxide interfaces on each restructured Au–Cu bimetallic nanoparticle. Au acts as the sites of CO adsorption and CuO_x provides the oxygen atom.

4.10 Au–Ni

Formation of surface alloy is one effective channel to tune surface composition and therefore catalytic performance.[38] One example is the ligand effect of alloyed Au atoms to nickel atoms. The Au atoms have an electron density that is more extended than that of the Ni atoms.[69,70] When the Au atoms are alloyed into the Ni surface layer, the Ni atoms next to an Au atom in the topmost layer experience a higher electron density or, equivalently, a larger effective coordination number. It can be considered that the Au atoms alloying with Ni atoms in the surface layer decreases the Ni surface energy of Ni atoms.[69,70] In fact, the charge transfer between a Au atom and its coordinating Ni atoms decreases the binding of carbon atoms to Ni atoms.[38] Therefore, binding of carbon atoms on Ni_xAu_{1-x} is weaker than pure Ni(111). The Ni_xAu_{1-x} can resist the formation of a coking layer and thus have a longer life than Ni catalysts.

On the other hand, this surface alloy restructures at high pressure of CO which is a product of the steam reforming of CH_4. STM studies showed that Ni can bind to CO to form nickel carbonyl which evaporates at room temperature. The "etching" starts at step edges. Upon the evaporation of $Ni(CO)_x$, Au islands are formed. The etching rate actually depends on the pressure of CO. The statistical accounting reveals the kinetics of the restructuring in the process.[92]

The thermodynamic factor in this de-alloying is very clear. Although Au has low surface energy in contrast to Ni, CO strongly binding to Ni is the main driving force for such a de-alloying. This study showed that evaporation of a metal in the formation of carbonyl is actually one potential channel to de-alloy or restructure a bimetallic surface.

4.11 Pt–Cu

Pt–Cu forms a near surface alloy by deposition of Cu or Pt followed by an annealing.[93,94] Surface restructuring of PtCu bimetallic nanoparticles (~2 nm) in H_2 and CO was studied using X-ray absorption near edge spectroscopy (XANES), Fourier transform infrared spectroscopy (FTIR) and pair distribution function analysis (PDF).[93] In an environment of CO, the Pt of PtCu nanoparticles segregated to the surface and Cu migrated to the core. This probably results from the larger

adsorption energy of CO on Pt atoms in contrast to Cu atoms. However, there is a reverse restructuring behavior in H_2. At 548 K in H_2, Cu segregates and forms a Cu-rich surface region. In this restructuring, probably the lower surface energy of Cu plays the major role. The restructuring behavior of 2 nm PtCu nanoparticles is different from that of PtCu surface alloy formed on a Pt single crystal.[93] For the Pt–Cu surface alloy formed on Pt single crystals in a CO environment, Cu in the sub-monolayer segregates to the surface and forms a Pt–Cu surface layer. This is driven by the stronger binding energy of CO on Pt coordinating with Cu compared to that on a pure Pt surface. The fully occupied Cu3d is expected to partially transfer electrons to the Pt4f, which enhances the back donation of electrons from Pt to the anti-π bond of a CO molecule.

4.12 Pt–Fe

Pt–Fe forms a surface alloy in a vacuum. The surface chemistry of PtFe surface alloys experiences changes under reaction conditions.[95] A PtFe surface alloy can be prepared with physical e-beam evaporation. Fe forms subsurface layers but Pt is located on the surface as a skin layer. Exposure to O_2 results in a surface segregation of Fe and the formation of FeO_x at a rather low pressure of O_2 (1×10^{-6} Torr). This process is reversible. In H_2, the FeO can be reduced and migrates to a subsurface layer. Upon the reduction of the oxide to Fe, Pt preferentially segregates to the surface since it has a lower surface energy. DFT calculations showed that (1) subsurface Fe is thermodynamically more stable in UHV and H_2 environments; and (2) the Fe–O bond is stronger than a Pt–O bond, consistent with experimental observation. The reversible restructuring is driven by the stronger Fe–O bond strength in contrast to that of Pt–O in an oxidizing environment and the low surface energy of Fe in reducing environments.

4.13 Pt–Co

Pt–Co is an intermetallic which is an important catalyst in several reactions. Pt and Co exhibit distinct capabilities upon being oxidized. Restructuring of Pt–Co thin films[96] and Pt–Co nanoparticles were studied. In UHV, they form a Pt–Co intermetallic. Pt preferentially segregates to the surface in hydrogen, forming a Pt shell. Pt–Co thin films and nanoparticles exhibit the same restructuring in H_2 (Fig. 10). However, the restructuring in O_2 is different for PtCo nanoparticles (Fig. 10) and PtCo thin films. Co in Pt–Co nanoparticles[96] is oxidized into CoO; but it is Co_3O_4 in the PtCo foil.[97]

4.14 Pt–Ni

Pt can form an alloy with Ni. Being one of the alloys formed from Pt and 3d metals, Pt segregates to the surface in reducing environments.[98] But in an oxidizing environment, Ni atoms preferentially form nickel oxide and thus block the segregation of Pt atoms to the surface.

4.15 Pt–Sn

Pt and Sn can form an alloy. The studies of Pt_3Sn alloy nanoparticles showed these nanoparticles restructure under reducing (H_2) or oxidizing (O_2) environments[99] in contrast to that in UHV. Their restructuring in H_2 is driven by the low

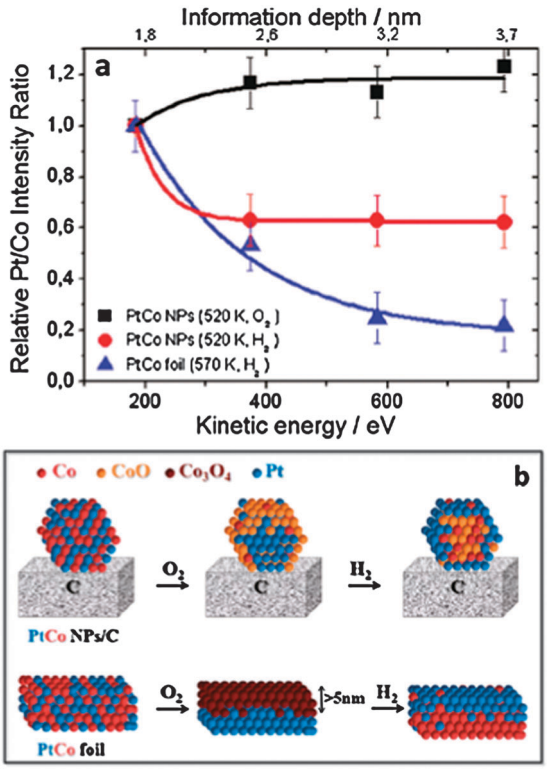

Fig. 10 (a) The Pt/Co atomic ratio calculated from the Pt 4f and Co 2p photoelectron peaks as a function of the electron kinetic energy, measured at 520 K for PtCo NPs in O_2 and in H_2 and for the PtCo foil in H_2. On the upper *x*-axis, the estimated average ID for each electron KE is given. (b) Schematic model illustration of the proposed PtCo atom arrangement in NPs and foil under oxidative and reductive environments.[96] (From ref. 96.)

surface energy of Pt and thus a Pt-rich surface is formed. However, in an oxidizing environment, Sn can be oxidized to form an oxide more easily in contrast to Pt. This is due to the high binding energy of oxygen atoms to Sn.

4.16 Pt–Ru

Pt–Ru is an important system for electrochemical oxidation of methanol in low-temperature fuel cells. It is impossible to examine the change in surface composition at the interface of the electrodes and fuel when such a fuel cell process is being performed. But fundamental studies of the potential restructuring are important in understanding the structural evolution during electrocatalysis. In addition, adding a certain amount of Ru was used to increase the tolerance to CO poisoning.

A computational study using a first-principle-based lattice gas Hamiltonian in grand-canonical Monte Carlo simulations was performed (Fig. 11).[100] Pt has a lower surface energy than Ru and is expected to segregate to the surface in UHV. However, in an oxidizing environment, the surface composition is quite different. This is because oxygen atoms can strongly bind to Ru in contrast to Pt, leading to an inversion of the segregation profile. With the increase of oxygen chemical potential due to an increase in oxygen pressure, Ru segregates to the surface gradually if the chemical potential of Ru is low. Notably, at low oxygen chemical potential Ru segregates to the

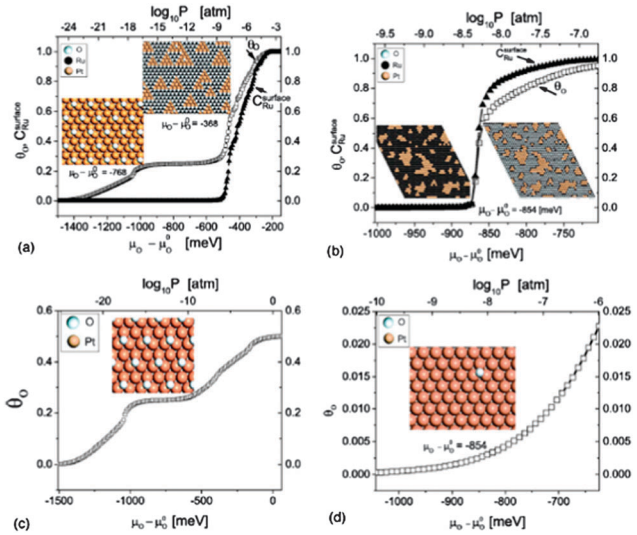

Fig. 11 Monte Carlo simulations and surface structure evolutions as a function of oxygen chemical potential μ_O, T and bulk Ru composition C_{Ru}. The conditions of (a) are $T = 600$ K, $\mu_{Ru} = -1750$ meV and (b) $T = 1050$ K, $\mu_{Ru} = -665$ meV. (c) and (d) are equilibrated oxygen isotherms at $T = 600$ K, and $T = 1050$ K in pure Pt surfaces with oxygen adsorbates.[100] (From ref. 100.)

surface in the form of isolated atoms. At higher oxygen chemical potential, the segregated Ru atoms form nanoclusters of the Ru atoms; the surface is different. Pt atoms form islands which are surrounded by oxygen-covered Ru regions.

5. Summary and prospects

Restructuring of surface regions of heterogeneous catalysts under reaction conditions or during catalysis is a phenomenon realized decades ago. However, it is certainly an under-represented field in heterogeneous catalysis due to certain reasons. One of the reasons is the lack of techniques capable of identifying surface chemistry and structure of catalysts under reaction conditions or during catalysis. Due to the availability of ambient pressure techniques for surface analysis in the past decade, many studies have been performed using these techniques. Numerous new chemistries of catalysts under reaction conditions or during catalysis were revealed. These studies certainly clarified many uncertainties about the "magic" of catalysis. More importantly, the identification of authentic surface chemistry and the structure of the active phase during catalysis offer first-hand insights for the design and optimization of catalysts. These new chemistries are encouraging more efforts to be made in this field. We expect an exciting period in heterogeneous catalysis, with the understanding of catalysis through operando and *in situ* studies of catalysts toward the design of new catalysts, which is emerging due to the advance in ambient pressure techniques and the importance of catalysis in energy conversion.

More than half of heterogeneous catalytic reactions involve metal particles of various sizes. Formation of various bimetallic nanoparticles offers infinite opportunities due to the tunability of the surface structure and chemistry of bimetallic catalysts. Early applications were made in the early 1980s. Traditionally, the understanding of mechanisms of bimetallic catalysis is based on a correlation between surface structure and the chemistry of the catalysts before a reaction and measured catalytic performance. Due to different surface energies of metal elements and different adsorption energies of species on metal atoms, the surface structure and chemistry in terms of surface composition, atomic distribution, sites, and oxidation states under reaction condition are very likely different from those before catalysis or after catalysis.

Operando and *in situ* studies of the surface chemistry and structure of catalysts, particularly bimetallic catalysts, are probably still at the embryonic stage. We are facing several challenges. One is the challenge of ambient pressure techniques. Although a few *in situ* analytical techniques including AP-XPS, high pressure STM, and environmental TEM are available, new techniques are required. For example, surface analytical techniques with a high temporal resolution are necessary for studies of surface dynamics during catalysis. In addition, surface sensitive imaging techniques with high temporal resolution are critical to track dynamic changes in surface structure during catalysis; surface sensitive spectroscopy with high spatial resolution is necessary for identifying the evolution of surface chemistry at a specific location with an accuracy of tens of nanometres or better. A promising technique is the ambient pressure XPS imaging technique. In addition, a surface analytic technique studying surface structure and chemistry at a solid–liquid interface is required. This is actually very important for energy conversion processes occurring at solid–liquid interfaces including generation of hydrogen at the catalyst–water interface, the interfacial area of electrode materials, electrolyte, and fuel, and the interface in solar cell processes.

Other than the challenges in experiments and characterization techniques, how to integrate computational studies into operando experiments is another challenge. One advantage of computational studies in catalysis is to screen catalysts on a computer and provide guidance for designing new catalysts. How computation studies could predict the surface chemistry and structure of catalysts under reaction, is challenging. If the prediction can be done, a direct comparison of the predicted structure and chemistry of catalysts will allow the exclusion of candidates, narrow the focus, and thus design catalysts efficiently. One more challenge is how to integrate the capability and advantage of operando studies into the important catalytic processes of energy conversion. From the point of view of experiments, *in situ* and operando studies can contribute to the catalysis studies of energy sciences from the following aspects. One is the *in situ* and operando studies of the whole process of catalysis including pretreatment of catalysts, reaction during catalysis, and deactivation. Another is to build correlation between the surface chemistry and structure of catalysts of energy conversion and catalytic performance and energy efficiency. In addition, it is necessary to develop operando diagnosis techniques which can examine the energy conversion devices including fuel cells when energy conversion is being performed.

Acknowledgements

This work is supported by the Chemical Sciences, Geosciences and Biosciences Division, Office of Basic Energy Sciences,

Office of Science, U.S. Department of Energy under the grant DE-FG02-12ER1635, and ACS PRF.

References

1 G. A. Somorjai and Y. Li, *Introduction to surface chemistry and catalysis*, Wiley, 2010.
2 G. A. Somorjai, F. Tao and J. Y. Park, *Top. Catal.*, 2008, **47**, 1–14.
3 J. R. Renzas, W. Y. Huang, Y. W. Zhang, M. E. Grass, D. T. Hoang, S. Alayoglu, D. R. Butcher, F. Tao, Z. Liu and G. A. Somorjai, *Phys. Chem. Chem. Phys.*, 2011, **13**, 2556–2562.
4 S. Alayoglu, F. Tao, V. Altoe, C. Specht, Z. W. Zhu, F. Aksoy, D. R. Butcher, R. J. Renzas, Z. Liu and G. A. Somorjai, *Catal. Lett.*, 2011, **141**, 633–640.
5 F. Tao, M. E. Grass, Y. W. Zhang, D. R. Butcher, J. R. Renzas, Z. Liu, J. Y. Chung, B. S. Mun, M. Salmeron and G. A. Somorjai, *Science*, 2008, **322**, 932–934.
6 N. Toshima and T. Yonezawa, *New J. Chem.*, 1998, **22**, 1179–1201.
7 F. Tao, M. E. Grass, Y. W. Zhang, D. R. Butcher, F. Aksoy, S. Aloni, V. Altoe, S. Alayoglu, J. R. Renzas, C. K. Tsung, Z. W. Zhu, Z. Liu, M. Salmeron and G. A. Somorjai, *J. Am. Chem. Soc.*, 2010, **132**, 8697–8703.
8 A. R. Tao, S. Habas and P. Yang, *Small*, 2008, **4**, 310–325.
9 S. H. Joo, J. Y. Park, C.-K. Tsung, Y. Yamada, P. Yang and G. A. Somorjai, *Nat. Mater.*, 2009, **8**, 126–131.
10 B. Lim, M. Jiang, P. H. C. Camargo, E. C. Cho, J. Tao, X. Lu, Y. Zhu and Y. Xia, *Science*, 2009, **324**, 1302–1305.
11 Y. G. Sun and Y. N. Xia, *Science*, 2002, **298**, 2176–2179.
12 D. V. Talapin, J.-S. Lee, M. V. Kovalenko and E. V. Shevchenko, *Chem. Rev.*, 2010, **110**, 389–458.
13 C. Burda, X. B. Chen, R. Narayanan and M. A. El-Sayed, *Chem. Rev.*, 2005, **105**, 1025–1102.
14 C. Rameshan, W. Stadlmayr, C. Weilach, S. Penner, H. Lorenz, M. Haevecker, R. Blume, T. Rocha, D. Teschner, A. Knop-Gericke, R. Schloegl, N. Memmel, D. Zemlyanov, G. Rupprechter and B. Kloetzer, *Angew. Chem., Int. Ed.*, 2010, **49**, 3224–3227.
15 C. Rameshan, C. Weilach, W. Stadlmayr, S. Penner, H. Lorenz, M. Havecker, R. Blume, T. Rocha, D. Teschner, A. Knop-Gericke, R. Schlogl, D. Zemlyanov, N. Memmel, G. Rupprechter and B. Klotzer, *J. Catal.*, 2010, **276**, 101–113.
16 M. S. Chen, D. Kumar, C. W. Yi and D. W. Goodman, *Science*, 2005, **310**, 291–293.
17 M. Salmeron and R. Schlogl, *Surf. Sci. Rep.*, 2008, **63**, 169–199.
18 F. Tao and M. Salmeron, *Science*, 2011, **331**, 171–174.
19 F. Tao, S. Dag, L. W. Wang, Z. Liu, D. R. Butcher, H. Bluhm, M. Salmeron and G. A. Somorjai, *Science*, 2010, **327**, 850–853.
20 M. S. Altman, *Science*, 2010, **327**, 789–790.
21 F. M. F. de Groot, E. de Smit, I. Swart, J. F. Creemer, G. H. Hoveling, M. K. Gilles, T. Tyliszczak, P. J. Kooyman, H. W. Zandbergen, C. Morin and B. M. Weckhuysen, *Nature*, 2008, **456**, 222–U239.
22 P. L. Hansen, J. B. Wagner, S. Helveg, J. R. Rostrup-Nielsen, B. S. Clausen and H. Topsoe, *Science*, 2002, **295**, 2053–2055.
23 T. W. Hansen, J. B. Wagner, P. L. Hansen, S. Dahl, H. Topsoe and C. J. H. Jacobsen, *Science*, 2001, **294**, 1508–1510.
24 D. Friebel, D. J. Miller, D. Nordlund, H. Ogasawara and A. Nilsson, *Angew. Chem., Int. Ed.*, 2011, **50**, 10190–10192.
25 J. T. Newberg, D. E. Starr, S. Yamamoto, S. Kaya, T. Kendelewicz, E. R. Mysak, S. Porsgaard, M. B. Salmeron, G. E. Brown, Jr, A. Nilsson and H. Bluhm, *Surf. Sci.*, 2011, **605**, 89–94.
26 F. Tao, M. Salmeron, J. Rodriguez and J. Hu, *ChemCatChem*, 2011, **3**, 1661–1662.
27 C. Wen, Y. Liu and F. Tao, *Pure Appl. Chem.*, 2011, **83**, 243–252.
28 F. Tao, *Chem. Commun.*, 2012, **48**, 3812–3814.
29 J. H. Sinfelt, *Bimetallic Catalysts*, John Wiley & Sons, 1983.
30 Y. Xiong, B. J. Wiley and Y. Xia, *Angew. Chem., Int. Ed.*, 2007, **46**, 7157–7159.
31 Y. Xia, Y. Xiong, B. Lim and S. E. Skrabalak, *Angew. Chem., Int. Ed.*, 2009, **48**, 60–103.
32 K. Jacobs, D. Zaziski, E. C. Scher, A. B. Herhold and A. P. Alivisatos, *Science*, 2001, **293**, 1803–1806.
33 Y. D. Yin, R. M. Rioux, C. K. Erdonmez, S. Hughes, G. A. Somorjai and A. P. Alivisatos, *Science*, 2004, **304**, 711–714.
34 H. Zheng, R. K. Smith, Y.-w. Jun, C. Kisielowski, U. Dahmen and A. P. Alivisatos, *Science*, 2009, **324**, 1309–1312.
35 M. T. Reetz and W. Helbig, *J. Am. Chem. Soc.*, 1994, **116**, 7401–7402.
36 K. Torigoe and K. Esumi, *Langmuir*, 1993, **9**, 1664–1667.
37 K. Torigoe, Y. Nakajima and K. Esumi, *J. Phys. Chem.*, 1993, **97**, 8304–8309.
38 F. Besenbacher, I. Chorkendorff, B. S. Clausen, B. Hammer, A. M. Molenbroek, J. K. Norskov and I. Stensgaard, *Science*, 1998, **279**, 1913–1915.
39 D. F. Ogletree, H. Bluhm, G. Lebedev, C. S. Fadley, Z. Hussain and M. Salmeron, *Rev. Sci. Instrum.*, 2002, **73**, 3872–3877.
40 M. E. Grass, P. G. Karlsson, F. Aksoy, M. Lundqvist, B. Wannberg, B. S. Mun, Z. Hussain and Z. Liu, *Rev. Sci. Instrum.*, 2010, **81**, 053106.
41 H. Bluhm, M. Haevecker, A. Knop-Gericke, M. Kiskinova, R. Schloegl and M. Salmeron, *MRS Bull.*, 2007, **32**, 1022–1030.
42 G. A. Somorjai, F. Tao and D. Butcher, in *Scanning Tunneling Microscopy in Surface Science*, ed. M. Bowker and P. R. Davies, Wiley, 2010, vol. 1, pp. 189–218.
43 A. Kolmakov and D. W. Goodman, *Rev. Sci. Instrum.*, 2003, **74**, 2444–2450.
44 E. Laegsgaard, L. Osterlund, P. Thostrup, P. B. Rasmussen, I. Stensgaard and F. Besenbacher, *Rev. Sci. Instrum.*, 2001, **72**, 3537–3542.
45 P. B. Rasmussen, B. L. M. Hendriksen, H. Zeijlemaker, H. G. Ficke and J. W. M. Frenken, *Rev. Sci. Instrum.*, 1998, **69**, 3879–3884.
46 M. Rossler, P. Geng and J. Wintterlin, *Rev. Sci. Instrum.*, 2005, **76**, 023705.
47 F. Tao, D. Tang, M. Salmeron and G. A. Somorjai, *Rev. Sci. Instrum.*, 2008, **79**, 084101.
48 F. Tao, S. Dag, L. W. Wang, Z. Liu, D. R. Butcher, M. Salmeron and G. A. Somorjai, *Nano Lett.*, 2009, **9**, 2167–2171.
49 L. Nguyen, F. Cheng and F. Tao, *J. Phys. Chem. C*, 2012, submitted.
50 A. I. Frenkel, Q. Wang, N. Marinkovic, J. G. Chen, L. Barrio, R. Si, A. Lopez Camara, A. M. Estrella, J. A. Rodriguez and J. C. Hanson, *J. Phys. Chem. C*, 2011, **115**, 17884–17890.
51 N. S. Marinkovic, Q. Wang, L. Barrio, S. N. Ehrlich, S. Khalid, C. Cooper and A. I. Frenkel, *Nucl. Instrum. Methods Phys. Res., Sect. A*, 2011, **649**, 204–206.
52 S. Helveg, C. Lopez-Cartes, J. Sehested, P. L. Hansen, B. S. Clausen, J. R. Rostrup-Nielsen, F. Abild-Pedersen and J. K. Norskov, *Nature*, 2004, **427**, 426–429.
53 H. Yoshida, Y. Kuwauchi, J. R. Jinschek, K. Sun, S. Tanaka, M. Kohyama, S. Shimada, M. Haruta and S. Takeda, *Science*, 2012, **335**, 317–319.
54 H. L. Xin, E. A. Pach, R. E. Diaz, E. A. Stach, M. Salmeron and H. Zheng, *ACS Nano*, 2012, **6**, 4241–4247.
55 S. B. Simonsen, I. Chorkendorff, S. Dahl, M. Skoglundh, J. Sehested and S. Helveg, *J. Catal.*, 2011, **281**, 147–155.
56 Z. Peng, F. Somodi, S. Helveg, C. Kisielowski, P. Specht and A. T. Bell, *J. Catal.*, 2012, **286**, 22–29.
57 J. A. Rodriguez, *Heterog. Chem. Rev.*, 1996, **3**, 17–32.
58 J. A. Rodriguez, *Surf. Sci. Rep.*, 1996, **24**, 225–287.
59 J. A. Rodriguez, *Surf. Sci.*, 1996, **345**, 347–362.
60 B. Sun, M. Qiao, K. Fan, J. Ulrich and F. Tao, *ChemCatChem*, 2011, **3**, 542–550.
61 M. E. Grass, M. Park, F. Aksoy, Y. Zhang, M. Kunz, Z. Liu and B. S. Mon, *Langmuir*, 2010, **26**, 16362–16367.
62 J. R. Renzas, W. Huang, Y. Zhang, M. E. Grass and G. A. Somorjai, *Catal. Lett.*, 2011, **141**, 235–241.
63 Y. M. Jin, A. K. Datye, E. Rightor, R. Gulotty, W. Waterman, M. Smith, M. Holbrook, J. Maj and J. Blackson, *J. Catal.*, 2001, **203**, 292–306.
64 L. Piccolo, A. Piednoir and J. C. Bertolini, *Surf. Sci.*, 2005, **592**, 169–181.
65 A. Hugon, L. Delannoy, J.-M. Krafft and C. Louis, *J. Phys. Chem. C*, 2010, **114**, 10823–10835.
66 J. R. Kitchin, K. Reuter and M. Scheffler, *Phys. Rev. B: Condens. Matter Mater. Phys.*, 2008, **77**, 075437.
67 J. Shu, B. E. W. Bongondo, B. P. A. Grandjean, A. Adnot and S. Kaliaguine, *Surf. Sci.*, 1993, **291**, 129–138.
68 S. Gonzalez, K. M. Neyman, S. Shaikhutdinov, H.-J. Freund and F. Illas, *J. Phys. Chem. C*, 2007, **111**, 6852–6856.
69 L. P. Nielsen, F. Besenbacher, I. Stensgaard and E. Laegsgaard, *Phys. Rev. Lett.*, 1995, **74**, 1159–1162.

70 L. P. Nielsen, F. Besenbacher, I. Stensgaard, E. Laegsgaard, C. Engdahl, P. Stoltze, K. W. Jacobsen and J. K. Norskov, *Phys. Rev. Lett.*, 1993, **71**, 754–757.
71 F. Gao, Y. Wang and D. W. Goodman, *J. Catal.*, 2009, **268**, 115–121.
72 F. Gao, Y. Wang and D. W. Goodman, *J. Phys. Chem. C*, 2009, **113**, 14993–15000.
73 F. Gao, Y. Wang and D. W. Goodman, *J. Am. Chem. Soc.*, 2009, **131**, 5734.
74 F. Gao, Y. Wang and D. W. Goodman, *J. Phys. Chem. C*, 2010, **114**, 4036–4043.
75 M. Garcia-Mota and N. Lopez, *Phys. Rev. B: Condens. Matter Mater. Phys.*, 2010, **82**, 075411.
76 H. Guesmi, C. Louis and L. Delannoy, *Chem. Phys. Lett.*, 2011, **503**, 97–100.
77 V. Soto-Verdugo and H. Metiu, *Surf. Sci.*, 2007, **601**, 5332–5339.
78 M. E. Grass, M. Park, F. Aksoy, Y. Zhang, M. Kunz, Z. Liu and B. S. Mon, *Langmuir*, 2010, **26**, 16362–16367.
79 T. C. Q. Noakes, P. Bailey, S. Laroze, L. H. Bloxham, R. Raval and C. J. Baddeley, *Surf. Interface Anal.*, 2000, **30**, 81–84.
80 J. A. Anderson, M. Lopez-Granados and M. Fernandez-Garcia, *J. Catal.*, 1998, **176**, 235–245.
81 N. Iwasa, S. Masuda, N. Ogawa and N. Takezawa, *Appl. Catal., A*, 1995, **125**, 145–157.
82 N. Iwasa, N. Ogawa, S. Masuda and N. Takezawa, *Bull. Chem. Soc. Jpn.*, 1998, **71**, 1451–1455.
83 K. Foettinger, J. A. van Bokhoven, M. Nachtegaal and G. Rupprechter, *J. Phys. Chem. Lett.*, 2011, **2**, 428–433.
84 W. Stadlmayr, C. Rameshan, C. Weilach, H. Lorenz, M. Haevecker, R. Blume, T. Rocha, D. Teschner, A. Knop-Gericke, D. Zemlyanov, S. Penner, R. Schloegl, G. Rupprechter, B. Kloetzer and N. Memmel, *J. Phys. Chem. C*, 2010, **114**, 10850–10856.
85 S. Linic, J. Jankowiak and M. A. Barteau, *J. Catal.*, 2004, **224**, 489–493.
86 J. T. Jankowiak and M. A. Barteau, *J. Catal.*, 2005, **236**, 366–378.
87 S. Linic, J. Jankowiak and M. A. Barteau, *J. Catal.*, 2004, **226**, 245–246.
88 S. Piccinin, S. Zafeiratos, C. Stampfl, T. W. Hansen, M. Haevecker, D. Teschner, V. I. Bukhtiyarov, F. Girgsdies, A. Knop-Gericke, R. Schloegl and M. Scheffler, *Phys. Rev. Lett.*, 2010, **104**, 035503.
89 S. Piccinin, C. Stampfl and M. Scheffler, *Phys. Rev. B: Condens. Matter Mater. Phys.*, 2008, **77**, 075426.
90 S. Piccinin, C. Stampfl and M. Scheffler, *Surf. Sci.*, 2009, **603**, 1467–1475.
91 X. Liu, A. Wang, L. Li, T. Zhang, C.-Y. Mou and J.-F. Lee, *J. Catal.*, 2011, **278**, 288–296.
92 E. K. Vestergaard, R. T. Vang, J. Knudsen, T. M. Pedersen, T. An, E. Laegsgaard, I. Stensgaard, B. Hammer and F. Besenbacher, *Phys. Rev. Lett.*, 2005, **95**, 126101.
93 S. M. Oxford, P. L. Lee, P. J. Chupas, K. W. Chapman, M. C. Kung and H. H. Kung, *J. Phys. Chem. C*, 2010, **114**, 17085–17091.
94 K. J. Andersson, F. Calle-Vallejo, J. Rossmeisl and L. Chorkendorff, *J. Am. Chem. Soc.*, 2009, **131**, 2404–2407.
95 T. Ma, Q. Fu, H.-Y. Su, H.-Y. Liu, Y. Cui, Z. Wang, R.-T. Mu, W.-X. Li and X.-H. Bao, *ChemPhysChem*, 2009, **10**, 1013–1016.
96 V. Papaefthimiou, T. Dintzer, V. Dupuis, A. Tamion, F. Tournus, D. Teschner, M. Haevecker, A. Knop-Gericke, R. Schloegl and S. Zafeiratos, *J. Phys. Chem. Lett.*, 2011, **2**, 900–904.
97 A. Borgna, B. G. Anderson, A. M. Saib, H. Bluhm, M. Havecker, A. Knop-Gericke, A. E. T. Kuiper, Y. Tamminga and J. W. Niemantsverdriet, *J. Phys. Chem. B*, 2004, **108**, 17905–17914.
98 R. Mu, Q. Fu, H. Liu, D. Tan, R. Zhai and X. Bao, *Appl. Surf. Sci.*, 2009, **255**, 7296–7301.
99 Y. Uemura, Y. Inada, K. K. Bando, T. Sasaki, N. Kamiuchi, K. Eguchi, A. Yagishita, M. Nomura, M. Tada and Y. Iwasawa, *J. Phys. Chem. C*, 2011, **115**, 5823–5833.
100 B. C. Han, A. Van der Ven, G. Ceder and B. J. Hwang, *Phys. Rev. B: Condens. Matter Mater. Phys.*, 2005, **72**, 205409.